Position Index Modulation for Fluid Antenna System

Halvin Yang, *Student Member, IEEE,* Hao Xu, *Member, IEEE,* Kai-Kit Wong, *Fellow, IEEE,* Chan-Byoung Chae, *Fellow, IEEE,* Ross Murch, *Fellow, IEEE,* Shi Jin, *Fellow, IEEE,* and Yangyang Zhang

***Abstract*—Fluid antenna system (FAS) represents all forms of movable and non-movable position-flexible antenna system, and opens up the possibility of a new form of modulation schemes. In this paper, we investigate the design of position index modulation (PIM) for FAS for decreasing the bit error rate (BER) while taking advantage of the rate gain in index modulation. We further derive the BER and data rate expressions to assess the achievable performance of PIM. Simulation results are provided to illustrate the performance and some insights are drawn into the impact of both channel estimation accuracy and transmission power.**

***Index Terms*—Bit error rate, data rate, fluid antenna system, index modulation, position index modulation.**

I. Introduction

A. Background

SPECTRAL efficiency has been one of the most important performance metrics for wireless communications. For the upcoming sixth generation (6G), it is predicted in [1] that the target will be 1000 bps/Hz. This will require multiple access technologies that permit spectrum sharing of a massive number of users while ensuring more information to be sent reliably over a physical channel. Several prominent technologies such as multiple-input multiple-output (MIMO) [2], reconfigurable intelligent surface (RIS) [3], non-orthogonal multiple access (NOMA) [4], are being studied to reach new limits.

Fluid antenna systems (FAS), proposed by Wong *et al.* [5], recently offer a new spectral-efficient solution. By adopting a 'fluid' antenna, a mobile receiver is capable of optimizing its position instantaneously and near-continuously over a predefined space. This differs from traditional selection combining in which signals are taken from fixed-position antennas with minimum distance of half wavelength apart. Physical design of fluid antennas might involve shifting soft materials (e.g., liquid metal, conductive fluid and others) using micro/nano-pumps [6] while other designs utilizing radio-frequency (RF) pixels are particularly attractive [7], [8], [9]. The former is suitable for positional change in seconds while the latter is ideal for positional change in microseconds or less. Latest experimental results regarding the implementation of FAS is given in [10], [11], showing promising results. There are also new advances in antenna design towards the concept of FAS, see [12], [13], [14]. Overall, FAS represents all forms of movable and non-movable shape-and-position flexible antenna system [15].

The work of Xu and Wong is supported by the Engineering and Physical Sciences Research Council (EPSRC) under Grant EP/W026813/1. For the purpose of open access, the authors will apply a Creative Commons Attribution (CC BY) licence to any Author Accepted Manuscript version arising.

The work of C. B. Chae is supported by the Institute of Information and Communication Technology Promotion (IITP) grant funded by the Ministry of Science and ICT (MSIT), Korea (No. 2021-0-02208, No. 2021-0-00486).

The work of R. Murch is supported by the Hong Kong Research Grants Council Area of Excellence grant AoE/E-601/22-R.

H. Yang, H. Xu, and K. K. Wong are with the Department of Electronic and Electrical Engineering, University College London, Torrington Place, WC1E 7JE, United Kingdom. K. K. Wong is also affiliated with Yonsei Frontier Lab, Yonsei University, Seoul, 03722, Korea.

C. B. Chae is with School of Integrated Technology, Yonsei University, Seoul, 03722, Korea.

R. Murch is with the Department of Electronic and Computer Engineering and Institute for Advanced Study (IAS), Hong Kong University of Science and Technology, Clear Water Bay, Hong Kong SAR, China.

S. Jin is is with the Frontiers Science Center for Mobile Information Communication and Security, Southeast University, Nanjing, China.

Y. Zhang is with Kuang-Chi Science Limited, Hong Kong SAR, China.

Corresponding author: K. K. Wong (e-mail: kai-kit.wong@ucl.ac.uk).

B. Related Work

The concept of FAS for wireless communications was first proposed in [5], in which the fundamental principles of fluid antenna aided communications were derived. The more ports (i.e., switchable positions) and/or the larger the electrical size of fluid antenna, the greater the performance. Since then, there has been strong interest in FAS. For example, [16] proposed approximations to characterize the full correlation structure of FAS for outage performance analysis. Recently, [17] presented some theoretical foundation of how a continuous FAS outperforms its discrete counterpart. Later, [18] also studied coded modulation designs using FAS. Efforts have also been made to understand the diversity gain of FAS [19], [20]. Additionally, there were attempts to extend the analysis to Nakagamai fading channels [21], [22], the α-μ channels [23] and arbitrary fading channels [24]. Recent research also looked into systems with multiple fluid antennas [25], [26], [27], [28].

Channel estimation in FAS is an important problem which is essential to provide the channel state information (CSI) for FAS to perform, and has recently been studied in [29], [30], [31]. Furthermore, the performance of FAS with outdated CSI was investigated in [32]. Recently, [33] developed a learning-based approach to select the best position for FAS in dynamic environments. FAS exploiting only statistical CSI, instead of instantaneous CSI, was given in [34]. The benefits of FAS for full duplex communications were also reported in [35].

Multiuser communications utilizing FAS was also recently studied. In [36], [37], [38], the authors studied the so-called *slow* fluid antenna multiple access (FAMA) which used FAS at each mobile user to switch to the best position for maximizing the average signal-to-interference plus noise ratio (SINR) for multiple access during a coherence time. Others contemplated the scenarios where each user's FAS was switched to the best position instantaneously on a per-symbol basis for superior

interference rejection capability [39], [40]. Most recently, the use of FAS was also considered to mix with NOMA [41], [42] and other information-theoretic schemes [43]. Additionally, a variation of FAMA for massive access was proposed in [44].

Despite the fast-growing results in FAS, code design benefiting from the flexible antenna structure is not well explored. In this regard, index modulation (IM) appears to be a great fit to FAS [45]. IM enables additional information to be carried by activating different aspects of communication resources, such as carriers [46], time slots [47] or antennas [48]. It can be combined with other technologies, e.g., orthogonal frequency division multiplexing (OFDM) [50] and is a widely recognized modulation technique that can be applied to many aspects of communications [49]. IM has already been considered with other emerging technologies, for example in conjunction with RIS. This concept was first proposed by Basar *et al.* in [51] and named as reflective IM (RIM). The technique in [52] divided the RIS elements into different groups and assigned each group an index. This could be improved by assigning an index to a different number of activated groups for improving the overall data rate since having different numbers of activated groups results in significantly different power signatures making demodulation less prone to error. Recently, [53] further expanded on how RIM can be deployed by proposing a multiple access IM scheme, with the RIS elements being configured to facilitate different indices simultaneously. A fluid antenna based index modulation for MIMO was most recently proposed in [54] which used an efficient sparse Bayesian detector.

Motivated by this, we propose a novel IM scheme, which we refer to it as position IM (PIM) utilizing a transmit FAS. This scheme exploits the unique nature of FAS and the presence of switchable ports to transmit additional information. Note that IM is normally employed in conjunction with some traditional modulation schemes such as OFDM [55], etc. Here we use IM together with quadrature amplitude modulation (QAM) or phase shift keying (PSK) to further increase the data rate.

C. Motivation and Contributions

IM can improve the performance of a wireless communication system, by providing an additional transmission domain which in turn increases the number of bits transmitted. This may result in an increase in error probability during demodulation which will be investigated. Utilizing the unique nature of FAS, new forms of IM are available which can be employed in conjunction with traditional modulation schemes to increase the number of bits able to be transmitted further. Due to the usage of FAS ports as indices for modulation, this requires a different usage of ports than that of previous research. Note that previous methods of always selecting the port that will result in the highest received signal power may not be possible due to the allocation of ports to indices – the optimal port for transmission may not be within the index group. This poses a key challenge of balancing the increased bits being transmitted with the decrease in signal quality as the error will increase from using a suboptimal port for transmission.

There are some similarities between PIM and spatial modulation (SM), the latter of which is another form of IM that assigns its index based on the position of fixed transmit antennas [56]. Technically both exploit the spatial difference of the radiating elements at the transmitter side to modulate additional data. However, most literature on SM considered non-correlated channels [57], [58], [59], although some analysis of correlated fading channels has also been done based on the Kronecker correlation model [60], [61]. Different from [60] and [61], our analysis is based on the channel model proposed in [40], which has been proven to accurately characterize the spatial correlation among the FAS ports. Furthermore, instead of simply selecting one of the transmit antennas, the proposed PIM scheme groups ports and then performs a further port selection process to identify the specific port radiating within the active port index group. Depending on the efficacy of port selection, this can affect the performance of PIM greatly.

Recently there have been other works designing IM for fluid antennas. However, the model in [54] requires multiple fluid antennas at the transmitter side to perform IM and hence needs more RF chains while in contrast our work operates needing only one fluid antenna at the transmitter side for PIM. Also, the work in [66] considers only one fluid antenna at the transmitter and employs coding to enhance system performance. But the results in [66] are only limited to rich-scattering Rayleigh fading channels. This means that the results in [66] would be inapplicable to the millimeter-wave or higher frequency bands where scattering is few. Furthermore, [66] states that the proposed coded IM has a particularly poor performance at low orders of IM, which is a notable issue since the majority of IM is aimed to operate at low orders. As such, both [66] and [54] suffer from significant restriction: the order of IM is restricted by the physical properties of the transmitter. This is particularly notable for [66] since the number of ports is equal to the modulation index. In a fluid antenna, it is common to have several hundred ports, resulting in high demodulation errors due to the spatial proximity and similarity of adjacent ports as well as a high computational complexity associated with computing so many indices. It is more desirable to have a dynamically adjustable IM order in order to adjust to the current channel conditions. This motivates our work to address these issues with the proposed PIM scheme.

This paper has made the following contributions:

- We propose a novel form of IM: PIM which uses ports as an index for conveying information. Desirably, the order of PIM can be dynamically changed during communications using the new idea of port grouping and the order is not restricted by the physical properties of the antenna. To facilitate port grouping, a new method of port selection is proposed, which selects the optimal port in each port group based on the greatest Euclidean distance on the constellation diagram. Since PIM can operate in conjunction with existing amplitude-phase modulation schemes such as QAM or PSK, we develop a novel transceiver architecture for enabling this.
- Analysis is done for a more general channel that works for scenarios with and without line-of-sight (LoS) paths and with any degree of scattering in the environment. This makes the analysis applicable for all frequency bands.
- The bit-error-rate (BER) of this joint modulation is ana-

lyzed to evaluate the impact of increasing the number of bits in PIM for this FAS architecture. Moreover, to get a better idea of the overall performance of PIM, the data rate is derived to see the impact of both the BER and increased bits in transmission.
- Simulation results show that our proposed port grouping method and PIM obtain significant performance increases over similar schemes or technologies indicating the importance of port grouping and the port selection algorithm when performing port-based IM.

The rest of this paper is organized as follows. Section II introduces the fundamental operating principle of PIM, which is followed by the system model and transceiver architecture in Section III. Performance analysis of BER and data rate is conducted in Section IV. After providing simulation results in Section V, our paper is concluded in Section VI.

II. Fundamental Principle of PIM

In a PIM-enhanced communication system, the information data is modulated in the port domain as well as the conventional phase-amplitude domain, as detailed below.

- Phase-Amplitude Domain: Standard modulation schemes like M-PSK or M-QAM are used for modulation in the phase-amplitude domain. For a modulation order M, the number of bits delivered during each transmission can be expressed as $K_{\mathrm{c}} = \log_2 M$, where the subscript 'c' indicates that it is the conventional modulation scheme.
- Port Domain: All ports on the FAS are separated into L groups. For a total number of P ports, each group contains $N_L = P/L$ ports. Since it is impossible to have fractional port groups, P and L have to be selected so that L is a factor of P and N_L is an integer. This modulation scheme is called L-PIM. The data bits in the port domain are carried by activating different port groups. The l-th port group activating pattern is denoted by $\boldsymbol{a}_l = [a_{l,1}, a_{l,2}, \ldots, a_{l,N_L}]$, where $a_{l,n} = 0$ when $l \neq n$ and $a_{l,n} = 1$ when $l = n$. '1' indicates that a particular group of ports is activated. When a port group is active, there is a singular port within that port group. How the active port within the port group is selected will be investigated in Section III-D. Since there are a total of L different port group activation patterns, $K_{\mathrm{p}} = \log_2 L$ bits can be delivered in each transmission. The mapping is done via grey code to convert the port group activation pattern into port information bits as shown in Table I.

The transmitter should first perform amplitude-phase modulation, and then send a control signal to the FAS in order to determine which port group will be activated during the current data transmission. It is assumed that the FAS can be controlled perfectly and there will be no error to the control signal. By jointly using phase-amplitude modulation as well as PIM, $K = K_{\mathrm{c}} + K_{\mathrm{p}}$ bits can be delivered during each transmission. The total number of bits per symbol is

$$K = K_{\mathrm{c}} + K_{\mathrm{p}} = \log_2 M + \log_2 L. \tag{1}$$

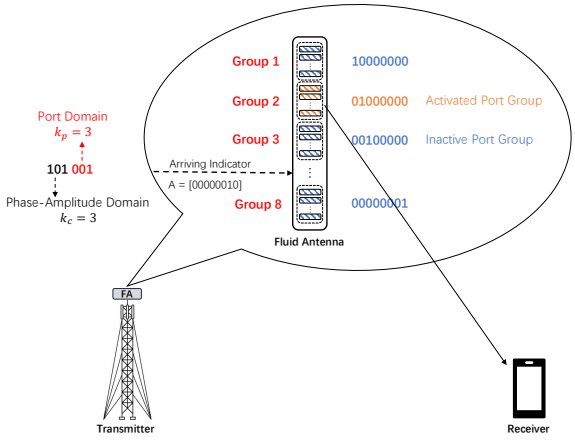

Fig. 1. The proposed architecture for a PIM-enhanced communication system using FAS at the transmitter side. As a point-to-point communication system is considered, the transmitter can be a handset but not a base station.

III. System Model and Transceiver Architecture

A. System Model

As shown in Fig. 1, we consider a PIM-assisted point-to-point communication system. The transmitter is equipped with a single fluid antenna with N ports while the receiver uses a conventional fixed-position antenna. The fluid antenna at the transmitter is capable of instantaneously switching to any port, only requiring one RF chain. It is assumed that there exists a LoS path between the FAS and the receiver as well as various non-line-of-sight (NLoS) paths.

A block fading channel is assumed between the transmitter and receiver, which is denoted as $\boldsymbol{h} \in \mathbb{C}^{1\times L}$ where L is the total number of position groups. The estimated CSI is destined to be imperfect, which is modelled as

$$\boldsymbol{h} = \rho\hat{\boldsymbol{h}} + \sqrt{1-\rho^2}\Delta\boldsymbol{h}, \tag{2}$$

where ρ is the accuracy parameter, $\hat{\boldsymbol{h}} \in \mathbb{C}^{1\times L}$ is the estimated channel vector, and $\Delta\boldsymbol{h} \in \mathbb{C}^{1\times L}$ represents the estimation error. Moreover, $\Delta\boldsymbol{h}$ consists of L independent and identically distributed (i.i.d.) Gaussian random variables, each with zero mean and variance of $\sigma_h^2 = d_{\mathrm{tr}}^{-\zeta}$, where d_{tr} is the distance between the transmitter and the receiver, and ζ is the path-loss exponent. Obviously, if $\rho = 1$, then the channel is perfectly estimated. Also, $\hat{\boldsymbol{h}} = [g_1, \ldots, g_L]$ is the channel between each port group of the FAS and the receive antenna. Since there are a total of N_L ports per group, a process is required to select a single active port from the N_L available ones. The process of obtaining the channel for a single active port, g_l, from all the available port channels, $g_{l,n}$, will be explained in Section III-D. The channel for a given port is modelled as [40]

$$g_{l,n} = \sqrt{\frac{K_{\mathrm{rice}}\Omega}{K_{\mathrm{rice}}+1}} e^{j\alpha} e^{-j\frac{2\pi(k-1)W}{N-1}\sin\theta_0\cos\phi_0} + \sum_{i=1}^{N_{\mathrm{p}}} \varphi_i e^{-j\frac{2\pi(k-1)W}{N-1}\sin\theta_i\cos\phi_i}, \tag{3}$$

where $g_{l,n}$ represents the n-th port in the l-th port group, $k = N_L(l-1)+n$, K_{rice} denotes the Rice factor, $\Omega = \mathbb{E}[|g_{n,l}|^2]$,

TABLE I
MODULATION PRINCIPLE OF 8-PIM

Port Pattern Index, l	Port Information Bits	Activated Group Number	Activating Indicator Vector, $\boldsymbol{a}_l$
1	000	1	$[1,0,0,0,0,0,0,0]$
2	001	2	$[0,1,0,0,0,0,0,0]$
3	011	3	$[0,0,1,0,0,0,0,0]$
4	010	4	$[0,0,0,1,0,0,0,0]$
5	110	5	$[0,0,0,0,1,0,0,0]$
6	111	6	$[0,0,0,0,0,1,0,0]$
7	101	7	$[0,0,0,0,0,0,1,0]$
8	100	8	$[0,0,0,0,0,0,0,1]$

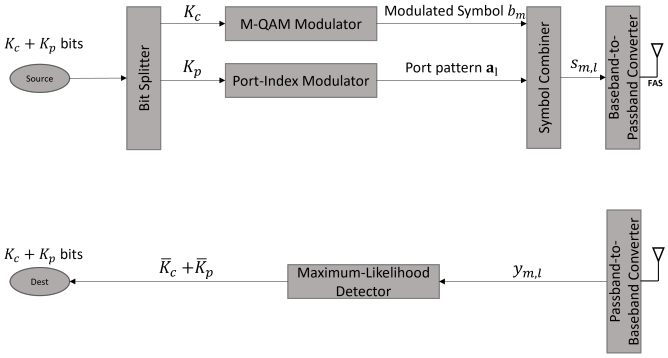

Fig. 2. The proposed transceiver architecture.

α is the random phase of the specular component, and φ_i is the complex coefficient of the i-th scattered path. Also, θ_i and ϕ_i are the azimuth and elevation angles of arrival (AoA), respectively. Finally, N_p is the number of NLoS paths.

For demodulation to occur, the receiver has to have knowledge of the constellation points of the modulated signal. As long as the number of ports present on the transmitting fluid antenna is known, the receiver can calculate which port within each port group is active by adopting the same port selection algorithm at the transmitter. Since the number of ports is a physical property, it cannot be changed and this value will be constant. After identifying the active ports within each port group, a constellation diagram can be constructed that would be identical to that employed by the transmitter. Although this adds some computational strain on the receiver, it offers the advantage of the receiver needing minimal information from the transmitter. Furthermore, for a stable block fading channel, this computation will only need to be done once every time the channel changes and the complexity is acceptable.

B. Transmitter Architecture

As shown in Fig. 2, the transmitter consists of the following modules:

- *Bit splitter:* This module splits the bit sequence from the source into phase-amplitude and port domains, which have the lengths of K_c and K_p bits, respectively.
- *M-QAM modulator:* This module maps K_c bits onto one modulated symbol b_m in the phase-amplitude domain with a baseband power of P_s.
- *Port-index modulator:* The port or position group which will be assigned for transmission is determined by the bit sequence of length K_p. A given K_p corresponds to a specific activating indicator vector $\boldsymbol{a}_l$ via Table I which will inform the fluid antenna which port group is active. Here the baseband port pattern $\boldsymbol{a}_l$ is generated.
- *Symbol combiner:* This module generates the integrated baseband symbol $s_{m,l} = \boldsymbol{a}_l b_m$.
- *Baseband-to-passband converter:* The combined baseband signal $s_{m,l}$ is converted to the RF band.

C. Receiver Architecture

As shown in Fig. 2, the receiver has the following modules:

- *Passband-to-baseband demodulator:* This module converts the received RF signal to the baseband ready for demodulation. Given the transmitted symbol $s_{m,l}$, the received signal $y_{m,l}$ can be expressed as

$$\begin{aligned} y_{m,j} &= \boldsymbol{h}\boldsymbol{a}_l^\mathrm{T} b_m + z \\ &= \rho\hat{\boldsymbol{h}}\boldsymbol{a}_l^\mathrm{T} b_m + \sqrt{1-\rho^2}\Delta\boldsymbol{h}\boldsymbol{a}_l^\mathrm{T} b_m + z \\ &= \rho g_l b_m + \sqrt{1-\rho^2}\Delta\boldsymbol{h}\boldsymbol{a}_l^\mathrm{T} b_m + z, \end{aligned} \tag{4}$$

  where z is the additive white Gaussian noise (AWGN) with zero mean and variance σ_z^2, and $g_j \triangleq \hat{\boldsymbol{h}}\boldsymbol{a}_l^\mathrm{T}$. Since the vector $\boldsymbol{a}_l$ contains only one non-zero term, it effectively selects the port group that is active, and the specific port within that port group will be outlined in Section III-D.
- *Maximum-likelihood (ML) detector:* This module outputs $\bar{K}_\mathrm{c} + \bar{K}_\mathrm{p}$ bits after the phase-amplitude demodulation of each symbol. The demodulation can be expressed as

$$(\bar{m}, \bar{l}) = \arg \min_{\substack{m' \in [1,\ldots,M] \\ l' \in [1,\ldots,L]}} |y_{m,l} - g_{l'} b_{m'}|^2, \tag{5}$$

  where $\bar{m}$ and $\bar{l}$ are the estimated indices of the M-QAM modulated symbol and the PIM symbol, respectively, and m' and l' are the trial indices.

D. Port Selection

Instead of selecting a single optimal port (as in a typical FAS), PIM port selection involves obtaining the vector $\boldsymbol{n}^*$, which contains L terms that detail the optimal port within each port group. For example, $\boldsymbol{n}^* = [n_1^*, n_2^*, n_3^*, n_4^*]$ containing the optimal port positions for 4-PIM modulation. When the second port group is being used, then the active port selected would be the n_2^*-th port in the second port group. The relationship between $\boldsymbol{n}^*$ and the selected active port k in (3) is given by

$$k = N_L(l-1) + n_l^*, \tag{6}$$

in which N_L is the number of ports in each port group. Port selection minimizes the chances of demodulation misidentifying any symbol, which is achieved by selecting ports whose constellation points are far apart. The main motivation behind using port groups rather than just finding the L ports in the whole fluid antenna is the reduction in computational complexity of the port selection process. Since the ports that are close spatially are highly correlated and are closer on the constellation diagram, there is no need to compare port pairs in close proximity. Therefore, by grouping ports that are adjacent together, the number of ports that need to be compared in the port selection process is significantly reduced.

In this paper, we propose three methods of port selection: (1) random selection, (2) signal-to-noise ratio (SNR) selection and (3) optimal selection.

(1) *Random selection:* This involves using a uniform random variable to select the port within each port group that will act as the active port.

(2) *SNR selection:* This selects the port with the highest SNR within the port group. More specifically, the SNR at the receiver when each port is used as the active transmitter is obtained and the port that results in the highest SNR at the receiver is selected. Note that this method requires to know the signal power at the receiver which may not always be possible. The optimal port position in the l-th group under this scheme is given by

$$n_l^* = \arg \max_{n\in[1,\ldots,N_L]} \{|g_{l,n}|\}, \tag{7}$$

where $g_{l,n}$ represents the n-th port in the l-th port group. Since there are a total of L port groups, the vector $\boldsymbol{n}^*$ which represents the optimal positions for all port groups is denoted by $\boldsymbol{n}^* = [n_1^*, n_2^*, \ldots, n_l^*, \ldots, n_L^*]$.

(3) *Optimal selection:* This is the proposed method in this paper. Here, the optimal port for each group is selected in such a way that the L total optimal ports have the greatest average Euclidean distance apart from each other on the constellation diagram. In theory, this is the best port selection method due to the use of an ML demodulator at the receiver. By maximizing the minimum distance between the selected positions, this reduces the probability of ML demodulation choosing an erroneous point in the received signal. For any given l, this can be achieved by

$$n_l^* = \arg \max_{n\in[1,\ldots,N_L]} \min_{\substack{\hat{l}\in[1,\ldots,L] \\ m,\hat{m}\in[1,\ldots,M] \\ \hat{n}\in[1,\ldots,N_L]}} |g_{l,n}b_m - g_{\hat{l},\hat{n}}b_{\hat{m}}|, \tag{8}$$

where n_l^* is the optimal port for the l-th port group and $l \neq \hat{l}$ or $m \neq \hat{m}$. Thus, $\boldsymbol{n}^* = [n_1^*, \ldots, n_l^*, \ldots, n_L^*]$ can be defined as the vector containing the optimal port for every group. The optimization in (8) is challenging. While exhaustive search is the most reliable way to obtain $\boldsymbol{k}^*$, this is only feasible for small N because the complexity increases exponentially. Since this problem is NP-hard, there are no easy solutions. This paper uses a genetic algorithm (GA) in order to obtain $\boldsymbol{n}^*$.

GAs are adaptive heuristic search algorithms inspired by natural selection. By going through successive iterative loops, called generations, GA can quickly narrow down regions where the optimal solution is located with the help of a fitness algorithm. The accuracy of the output of a GA can be determined by the tolerance, with a lower tolerance leading to a more accurate output. In this paper, the tolerance is set at 1×10^{-6} for a highly accurate output, and there is no restriction on the number of generations meaning that GA will keep going until no successive iterations differ by more than the tolerance. Due to the complexity of GA highly dependent on the population size as well as other factors like the crossover and mutation, it is impossible to quantify the complexity using a general expression. Therefore, Fig. 3 is used to compare the complexities of GA and exhaustive search under specific scenarios. As can be seen, for very low populations exhaustive search and GA have a similar complexity; however as the population increases it is clear that GA has a significantly higher efficiency.

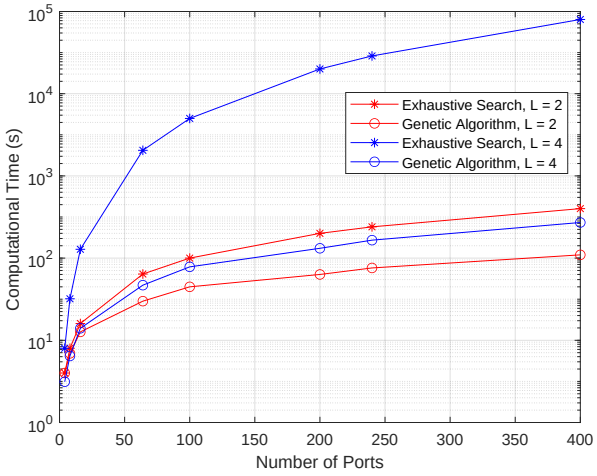

Fig. 3. Complexity of GA and exhaustive search for different numbers of ports and port groups.

Fig. 4 shows the constellation diagrams associated with the three different port selection schemes. As can be observed, the optimal selection scheme has all constellation points spread out with a uniform distance, while SINR selection and random selection have some constellation points which are in close proximity. From the diagram alone, it can be seen that the optimal selection scheme is the most effective in spreading out constellation points and therefore is likely to yield the lowest BER. The efficacy of each scheme is presented in Section V.

Three scenarios can be observed in regards to the number of port groups L as follows.

Case 1: When $L = 1$, this means that the number of ports is equal to the number of ports in each group ($N_L = P$). Since $K_\mathrm{p} = \log_2 L$, this effectively means there is no PIM present and the only modulation being done is phase-amplitude modulation. Port selection is therefore only needed to improve the signal power at the receiver, as performed in, e.g., [33].

Case 2: When $L = P$, then there is only a single port in each

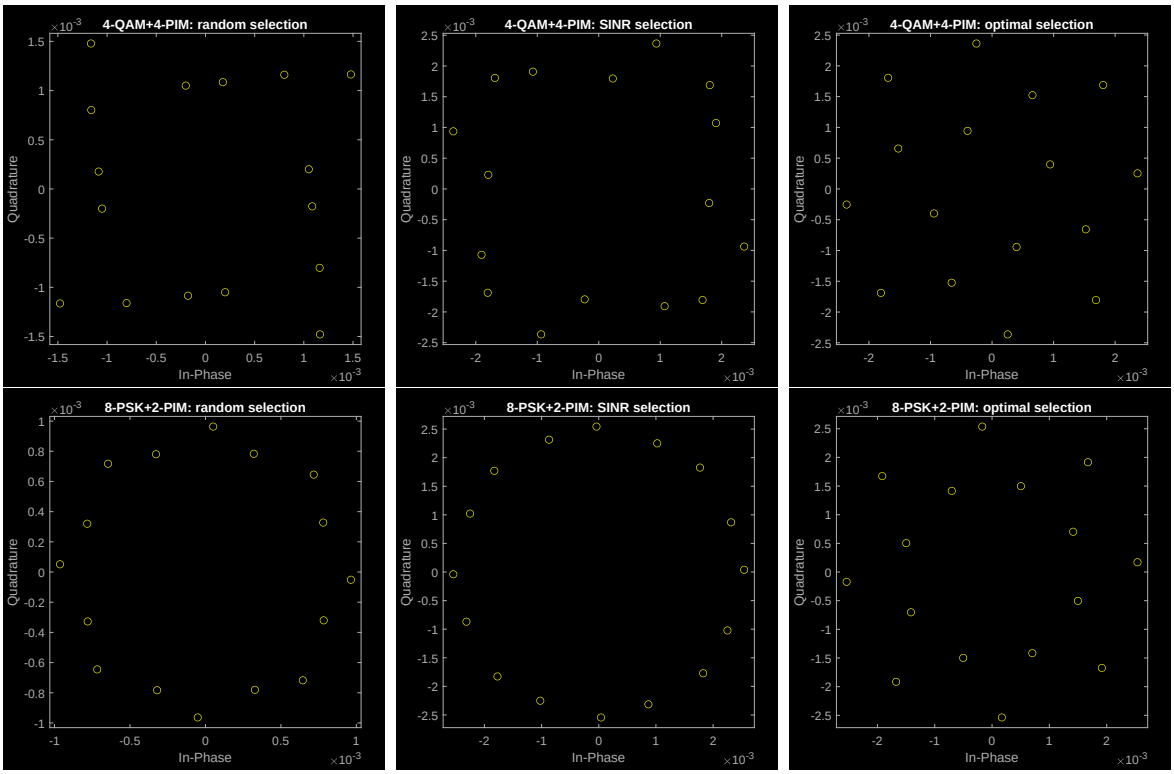

Fig. 4. Constellation diagrams of different port selection schemes: Random Selection (left), SNR selection (center), optimal selection (right).

group, and there is effectively no difference between ports and port groups. In this case, port selection is no longer required.

Case 3: When $L \neq 1$ and $L \neq P$, the base station transmitter can dynamically adjust the number of port groups to optimize the signal quality and the amount of data transmitted. Note that the number of port groups should be such that binary logarithm of the number of groups should be an integer.

IV. Performance Analysis

In this section, the BER of the PIM-assisted system is evaluated using the ML detection approach. In order to calculate the BER, the pairwise error probability (PEP) is first derived.

A. PEP

Firstly, we define the PEP between two joint symbols $s_{m,l}$ and $s_{n,p}$ for $m \neq n, l \neq p$ as $\tau(s_{m,l} \to s_{n,p})$, which is the probability that the Euclidean distance between the received signal $y_{m,l}$ and $s_{m,l}$ is larger than that between $y_{m,l}$ and $s_{n,p}$, when $s_{m,l}$ is transmitted. We have the following results.

Lemma 1: $\tau(s_{m,l} \to s_{n,p})$ can be expressed as

$$\begin{aligned}&\tau(s_{m,l} \to s_{n,p})\\ =&\Pr\left[|y_{m,l} - g_l b_m|^2 > |y_{m,l} - g_p b_n|^2\right]\\ =&\Pr\left[\begin{array}{c}|(\rho-1)\hat{\boldsymbol{h}}\boldsymbol{a}_l^{\mathrm{T}} b_m + \sqrt{1-\rho^2}\Delta\boldsymbol{h}\boldsymbol{a}_l^{\mathrm{T}} b_m + z|^2\\ > |\rho\hat{\boldsymbol{h}}\boldsymbol{a}_l^{\mathrm{T}} b_m + \sqrt{1-\rho^2}\Delta\boldsymbol{h}\boldsymbol{a}_l^{\mathrm{T}} b_m + z - g_p b_n|^2\end{array}\right].\end{aligned} \tag{9}$$

Theorem 1: The PEP can be further simplified into

$$\tau(s_{m,l} \to s_{n,p}) = Q\left(\frac{|\rho g_l b_m - g_p b_n|^2 - |(\rho-1) g_l b_m|^2}{\sqrt{2}\sigma_{m,l}|g_p b_n - g_l b_m|}\right), \tag{10}$$

where

$$Q(x) = \int_x^{+\infty} \frac{1}{\sqrt{2\pi}} e^{-\frac{t^2}{2}} dt. \tag{11}$$

Proof: Taking the result from Lemma 1, $\Delta\boldsymbol{h}$ is a vector containing L Gaussian distributed terms and independent of the noise z. Additionally, $\sqrt{1-\rho^2}\Delta\boldsymbol{h}\boldsymbol{a}_l^{\mathrm{T}} b_m + z$ is Gaussian distributed. By expressing $\lambda_{m,l} = \sqrt{1-\rho^2}\Delta\boldsymbol{h}\boldsymbol{a}_l^{\mathrm{T}} b_m + z$, we have a random variable $\lambda_{m,l} \sim \mathcal{CN}(0, \sigma_{m,l}^2)$, where $\sigma_{m,l}^2 = (1-\rho^2)\|\boldsymbol{a}_l\|^2 |b_m|^2 \sigma_h^2 + \sigma_z^2$. Thus, (9) can be rewritten as

$$\begin{aligned}&\tau(s_{m,l} \to s_{n,p})\\ =&\Pr\left[|(\rho-1) g_l b_m + \lambda_{m,l}|^2 > |\rho g_l b_m - g_p b_n + \lambda_{m,l}|^2\right] &(12)\\ =&\Pr\left[\begin{array}{c}2\mathrm{Re}\{\lambda_{m,l}(g_p b_n - g_p b_m)^*\}\\ > |\rho g_l b_m - g_p b_n|^2 - |(\rho-1) g_l b_m|^2\end{array}\right] &(13)\\ =&Q\left(\frac{|\rho g_l b_m - g_p b_n|^2 - |(\rho-1) g_l b_m|^2}{|g_p b_n - g_l b_m|\sqrt{2\sigma_{m,l}^2}}\right), &(14)\end{aligned}$$

where $\mathrm{Re}\{x\}$ denotes the real part of x. Also, $\mathrm{Re}\{\lambda_{m,l}(g_p b_n - g_p b_m)^*\}$ is Gaussian distributed, with properties $\mathcal{N}(0, |g_p b_n - g_l b_m|^2 \sigma_{m,l}^2/2)$. For further steps on how (13) is obtained from (12), please refer to Appendix A. ■

B. BER

Theorem 2: The BER can be approximated as

$$\epsilon \approx \frac{1}{K|\mathcal{S}|} \sum_{s_{m,l}\in\mathcal{S}} \sum_{s_{n,p}\in\mathcal{S}} d(s_{m,l}, s_{n,p}) \tau(s_{m,l} \to s_{n,p}), \quad (15)$$

where K is the total number of bits per symbol, see (1), $\mathcal{S}$ denotes the set containing all possible symbols, and $d(s_{m,l}, s_{n,p})$ is the Hamming distance between the symbols $s_{m,l}$ and $s_{n,p}$. This applies when the SNR is not too low. The probability $\Pr(s_{m,l} \to s_{n,p})$ can be approximated as the PEP [62].

Proof: The BER from decoding can be expressed as

$$\epsilon = \frac{1}{K|\mathcal{S}|} \sum_{s_{m,l}\in\mathcal{S}} \sum_{s_{n,p}\in\mathcal{S}} d(s_{m,l}, s_{n,p}) \Pr(s_{m,l} \to s_{n,p}), \quad (16)$$

which is the fundamental definition of BER [67] as an expression of the Hamming distance, and is the number of positions at which the two corresponding symbols are different, and the probability of misdemodulation. In (16), $\Pr(s_{m,l} \to s_{n,p})$ denotes the probability that $s_{m,l}$ is demodulated as $s_{n,p}$, which completes the proof. ■

The BER in Theorem 2 can be decomposed to obtain the BER of the phase-amplitude and port domains separately via the decomposition of the Hamming distance, which can be decomposed into $d(s_{m,l}, s_{n,p}) = d_{\mathrm{c}}(s_{m,l}, s_{n,p}) + d_{\mathrm{p}}(s_{m,l}, s_{n,p})$.

Lemma 2: The BER of the information bits in the phase-amplitude domain can be expressed as

$$\epsilon_{\mathrm{c}} \approx \frac{1}{K|\mathcal{S}|} \sum_{s_{m,l}\in\mathcal{S}} \sum_{s_{n,p}\in\mathcal{S}} d_{\mathrm{c}}(s_{m,l}, s_{n,p}) \tau(s_{m,l} \to s_{n,p}), \quad (17)$$

where $d_{\mathrm{c}}(\cdot,\cdot)$ is the Hamming distance between the information bits carried in the phase-amplitude domain.

Lemma 3: The BER of the information bits in the position or port domain can be expressed as

$$\epsilon_{\mathrm{p}} \approx \frac{1}{K|\mathcal{S}|} \sum_{s_{m,l}\in\mathcal{S}} \sum_{s_{n,p}\in\mathcal{S}} d_{\mathrm{p}}(s_{m,l}, s_{n,p}) \tau(s_{m,l} \to s_{n,p}), \quad (18)$$

where $d_{\mathrm{p}}(\cdot,\cdot)$ is the Hamming distance between the information bits carried in the port domain.

Fig. 5 shows the separate BER of PIM, QAM and PSK whilst considering an order of 4 for each. As can be observed, the BER as a result of the port domain is noticeably higher than that of the phase-amplitude domain.

C. Throughput Analysis

For PIM, the higher the number of port groups, the more the information bits to be transmitted but at the compromise of the BER. In order to gain further insight onto the relationship between the total number of modulation bits K and the BER, the system throughput can be observed.

Due to the usage of a ML detector for demodulation, the PEP between any pair of modulated symbols is symmetric. Therefore, the channel between the transmitter and receiver can be modelled as a memoryless binary symmetric channel. The mutual information between an input bit $x \in \{0,1\}$ and the estimated output bit $\bar{y} \in \{0,1\}$ can be found by

$$I(x;\bar{y}) = H(\bar{y}) - H(\bar{y}|x), \quad (19)$$

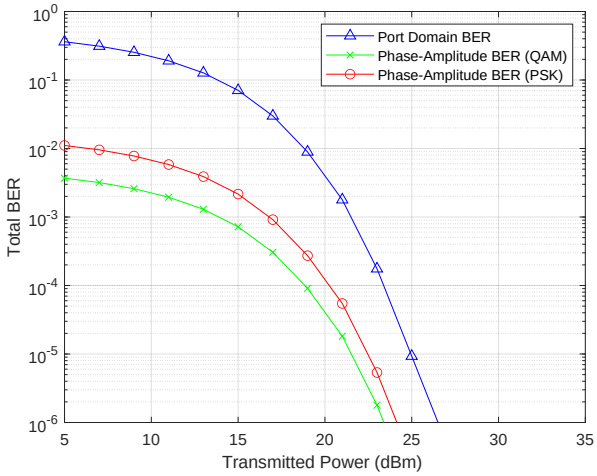

Fig. 5. Comparison of the separate BER of each modulation type.

where $H(\cdot)$ is the entropy function.

Lemma 4: $H(\bar{y})$ can be expressed as

$$\begin{aligned} H(\bar{y}) = &-(p_{x0}(1-\epsilon) + p_{x1}\epsilon)\log(p_{x0}(1-\epsilon) + p_{x1}\epsilon) \\ &- (p_{x1}(1-\epsilon) + p_{x0}\epsilon)\log(p_{x1}(1-\epsilon) + p_{x0}\epsilon), \end{aligned} \quad (20)$$

where p_{x0} and p_{x1} are respectively the probabilities that x is 0 and 1.

Proof: $H(\bar{y})$ can initially be expressed as

$$\begin{aligned} H(\bar{y}) &= -p_{\bar{y}0}\log(p_{\bar{y}0}) - p_{\bar{y}1}\log(p_{\bar{y}1}) \\ &= -(p_{x0}p_{\bar{y}0|x0} + p_{x1}p_{\bar{y}0|x1})\log(p_{x0}p_{\bar{y}0|x0} + p_{x1}p_{\bar{y}0|x1}) \\ &\quad - (p_{x0}p_{\bar{y}1|x0} + p_{x1}p_{\bar{y}1|x1})\log(p_{x0}p_{\bar{y}1|x0} + p_{x1}p_{\bar{y}1|x1}), \end{aligned} \quad (21)$$

where $p_{\bar{y}0}$ and $p_{\bar{y}1}$ are the probabilities of the estimated output being 0 and 1, respectively, and $p_{\bar{y}a|xb}$ is the probability that $x = b$ is decoded as $y = a$. Since this is a binary symmetric channel, $p_{\bar{y}0|x1} = p_{\bar{y}1|x0} = \epsilon$, where ϵ is the BER. By using this, (21) can be reformulated as (20). ■

Lemma 5: The entropy $H(\bar{y}|x)$ is

$$H(\bar{y}|x) = -\epsilon\log\epsilon - (1-\epsilon)\log(1-\epsilon). \quad (22)$$

Proof: Due to the symmetric nature of the channel, by assuming that $p_{x0} = p_{x1} = 0.5$ and substituting into (20), the entropy of the channel output $H(\bar{y}) = 1$. When the channel output is 1, the noise entropy can be derived as

$$H(\bar{y}|x) = -\sum_{b\in\{0,1\}} p_{xb} \sum_{a\in\{0,1\}} p_{\bar{y}a|xb}\log(p_{\bar{y}a|xb}), \quad (23)$$

which simplifies to (22). ■

Finally, by combining Lemma 4 and Lemma 5 the data rate can be obtained using the following theorem.

Theorem 3: The achievable data rate per transmission can be expressed as

$$R = KI(x;\bar{y}) = K(1 + \epsilon\log\epsilon + (1-\epsilon)\log(1-\epsilon)), \quad (24)$$

where K is the total bits carried by the modulated symbol.

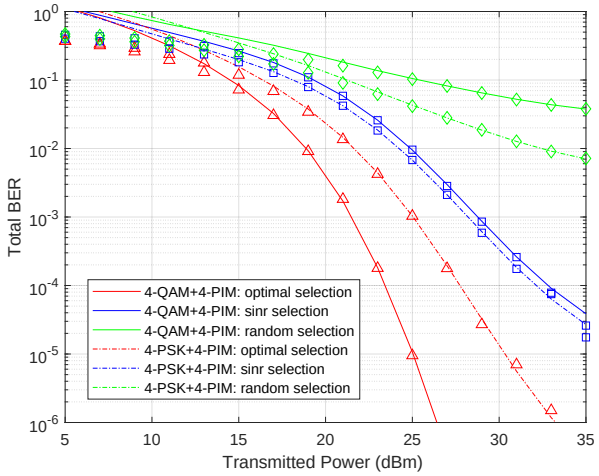

Fig. 6. Analytical results (lines) and Monte Carlo simulations (points) for different modulation schemes and port selection algorithms.

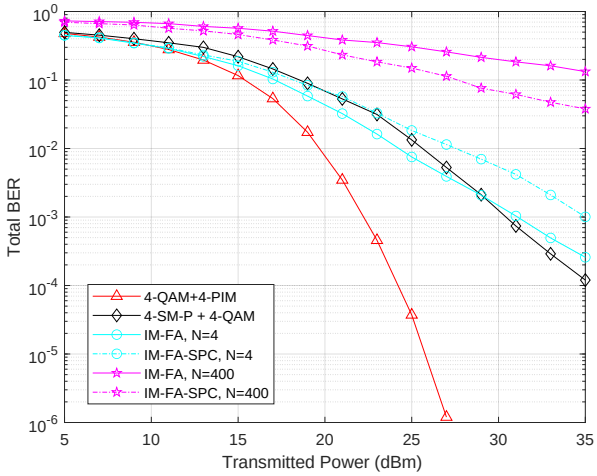

Fig. 7. Comparison of the Monte Carlo simulations for optimal port selection scheme with other similar modulation schemes.

V. Numerical Results and Discussion

Here, the performance of a joint PIM modulated system is validated by both Monte Carlo simulations and our analytical results. The channel model used has been described in Section III which consists of a LoS path with a Rice factor of $K_{\text{rice}} = 7$ and a total of $N_{\text{p}} = 2$ non-LoS paths. The width of FAS is assumed to be $W = 10$ wavelengths in size.

A. Validation

Fig. 6 compares the analytical results against the Monte Carlo simulations. A total of $N = 400$ ports were used with the AWGN power being -50 dBm and the channel estimation having an accuracy of $\rho = 0.999$. The simulation results (points) and our derived results (line) are very close together, showing the accuracy of our derivations. However, there are some differences between the simulation and derivations when the transmission power is less than 15 dBm which shows the limitation of the analysis done in this paper. Since index modulation is normally done at higher transmission powers, this is not a significant issue as normally the transmission power would be much larger than 15 dBm.

Furthermore, as the transmission power increases, the BER decreases. This is expected because the larger the signal power the higher the SNR resulting in the ML demodulator being able to identify different symbols more clearly. This result conforms to the expected result and indicates the correctness of the simulation and numerical results. It can also be noted that under the same PIM order of $L = 4$, QAM outperforms PSK by a large margin showing that QAM is the more suitable phase-amplitude modulation to be used with PIM.

Fig. 7 compares the performance of PIM with that of similar modulation schemes, namely SM and other fluid antenna IM schemes. The phase-only pre-scaling (SM-P) model in [63] has been shown to have significantly better performance than conventional SM and will be used for comparison. The fluid antenna IM in [66] will also be used as a benchmark since it outperforms the model given in [54]. To fit the scenario of PIM, a multiple-input single-output (MISO) system containing 4 transmit antennas is considered for SM adopting the SM-P model. For the benchmark IM scheme, two variations of IM found in [66] are used for comparison: index modulated FA with set partition coding (IM-FA-SPC) and without any coding (IM-FA). Two scenarios for IM-FA were considered: a scenario where the number of bits modulated by both methods was the same, and a scenario where the total number of ports present were the same. For the former scenario, a total of 4 data bits would be modulated in conjunction with IM and QAM. The order of IM would be the same in this comparison, with the number of ports $N = 4$ for IM-FA-SPC and IM-FA while the number of port groups is $L = 4$ for PIM. In the latter scenario, a total of $N = 400$ ports would be considered. For fair comparison, the size of the fluid antenna was changed to be 1.5λ in length, as otherwise IM-PIM would not have any correlation between ports, and $K = 0$ was set for PIM in order to match the Rayleigh fading channel model used in [66].

As observed in Fig. 7, 4-PIM has better performance than SM-P which shows its viability over traditional fixed-position antenna modulation schemes. Furthermore, the results indicate that PIM has better performance than both IM-FA and IM-FA-SPC for modulating the same number of bits and much better BER performance when considering the same number of ports. Interestingly, IM-FA-SPC seems to have worse performance than IM-FA at low number of ports. This is due to IM-FA-SPC having a lower modulation order compared to IM-FA by 1, meaning that QAM has to modulate an additional bit while at low correlation the effect of SPC coding is not very noticeable. This is similar to the results reported in [66] and backs the correctness of the simulation results. These simulation results show that the port grouping method proposed in this paper significantly improves the BER performance.

B. Comparison of Port Selection Schemes

The effectiveness of different port selection schemes in Section III is studied by the results in Fig. 8 under the same parameters as before. The modulation used in conjunction

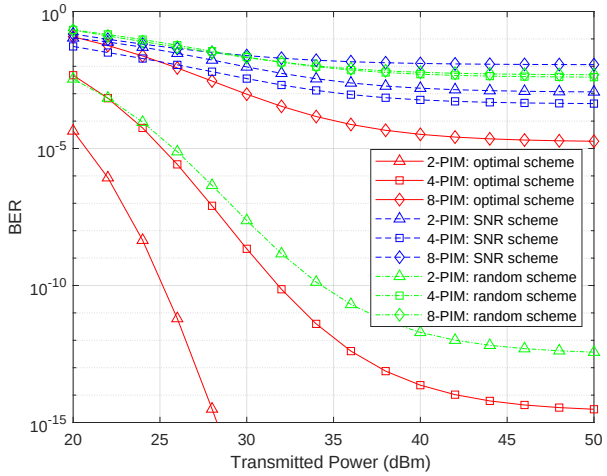

Fig. 8. Comparison of the three port selection algorithms for different number of bits modulated by PIM while observing BER.

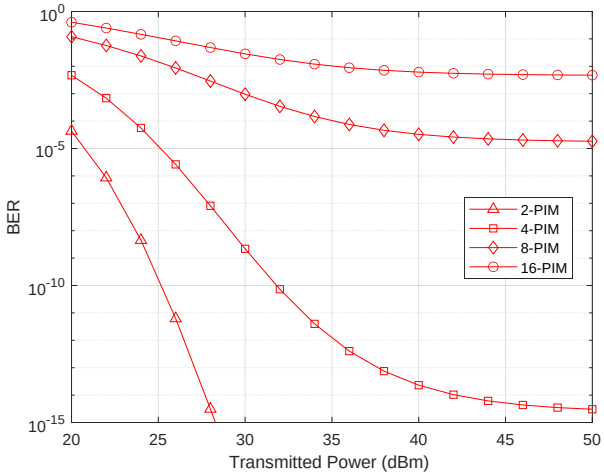

Fig. 10. The impact of L-PIM on BER.

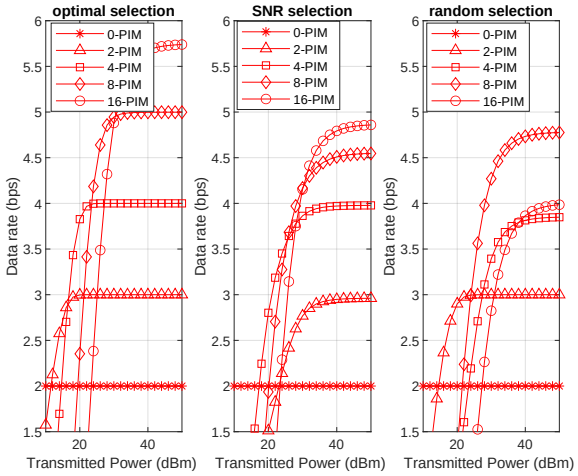

Fig. 9. Comparison of the three port selection algorithms for different number of bits modulated by PIM while observing data rate.

with L-PIM is 4-QAM. As can be seen, the proposed optimal port selection scheme outperforms both random selection and SINR selection significantly; 4-PIM with optimal selection even outperforming 2-PIM with the other selection algorithms. This shows the importance of port selection in PIM, as with the correct algorithm more bits can be transmitted while still having a lower BER. As expected, the lower the number of bits modulated by PIM, the lower the BER. However, BER does not tell the full story as even though the error rate is higher more bits are being transmitted which may result in an overall higher amount of correct data received.

On the other hand, data rate looks at the overall data received whilst also considering the impact of BER. The initial observations that can be made from Fig. 9 are that SINR selection slightly outperforms random selection when $L > 4$. Once again, the proposed optimal selection algorithm significantly outperforms its counterparts; the data rate saturates at a lower transmission power and in the case of no saturation the data rate is higher. These results offer insight on which port selection to use in what situation. If optimal selection is not available due to computational limitations, random selection should be used for $L \leq 4$ and SINR selection should be used for $L \geq 8$. Furthermore, it is interesting to note that at low powers, adding PIM on top of 4-QAM acts as a detriment to the performance of the system. 0-PIM represents only having 4-QAM modulation (hence the data rate is a constant 2, due to 4-QAM modulating 2 bits). The transmission powers at which L-PIM in the respective port selection schemes results in a gain in data rate can be observed in the figure as the point at which the PIM line crosses the base 4-QAM line.

C. Increasing Modulation Order

From previous results, it can be seen that an increase in PIM has an impact on the BER. Fig. 10 investigates this further, where 4-QAM modulation is used in conjunction with L-PIM. As expected, as L increases so does the BER. This is expected, as the more points there are on the constellation diagram the more likely ML demodulation will get it wrong. As L doubles to facilitate the modulation of an extra bit, there are 4 times more points on the constellation diagram. Also, for higher modulation like 8-PIM or 16-PIM, the BER begins to saturate at around power of 40 dBm, after which increasing transmission power does not have a significant impact on the BER. If using 8 or 16-PIM in a communication system, the signal power does not need to be higher than 40 dBm. This trend likely extends for $L \geq 16$; however even at 16-PIM, the BER is very high and going any higher is not advisable. A balance needs to be struck between the signal quality and the data rate. In particular, coding more bits will result in a higher BER and L in L-PIM and that will have to depend on the demands of a particular communication system.

As before, to get a more rounded view of the performance of L-PIM, we observe the data rate in Fig. 11. Once again, it can be seen that at low transmission power, PIM should not be used as it underperforms a traditional 4-QAM system with no PIM. The transmission that PIM should be used is dependant

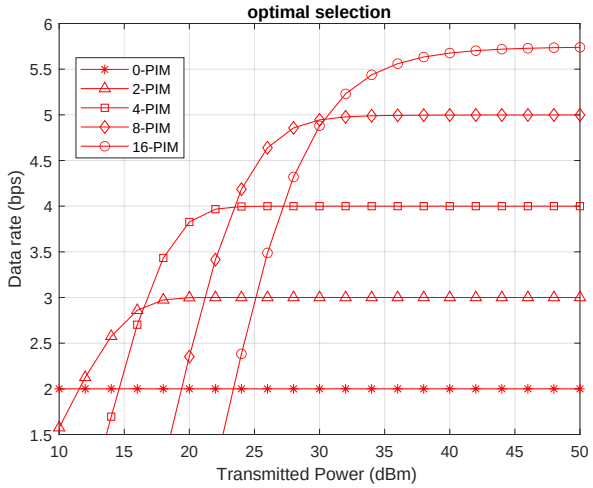

Fig. 11. The impact of L-PIM on data rate.

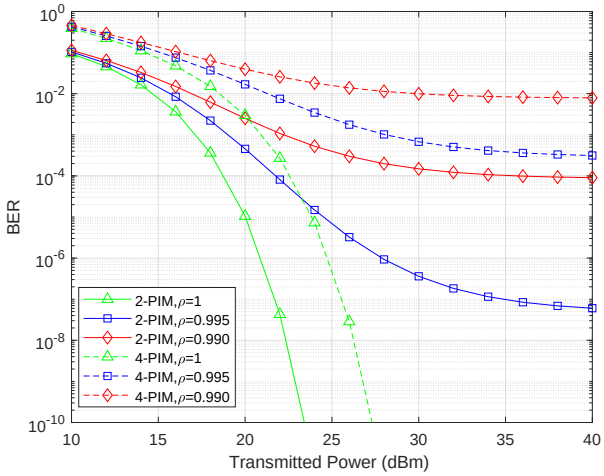

Fig. 13. BER for PIM-4-QAM with different CSI accuracy.

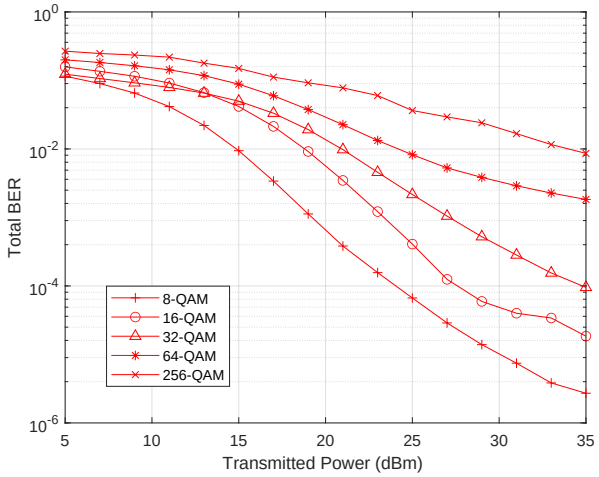

Fig. 12. Comparison of higher orders of QAM in conjunction with 2-PIM

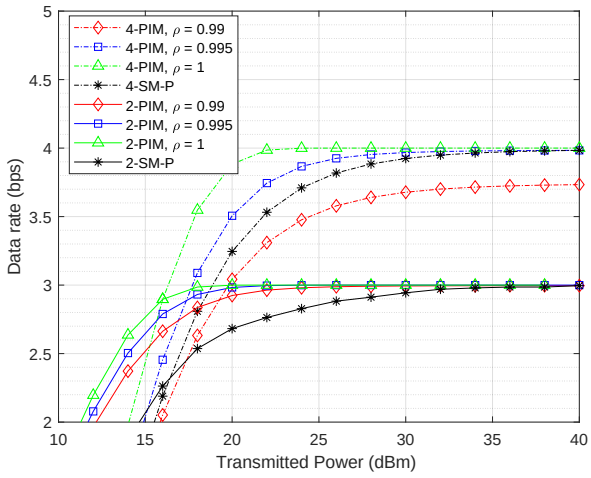

Fig. 14. Data rate for PIM-4-QAM with different CSI accuracy and comparison to benchmark scheme.

on the number of bits being modulated by PIM, with 12 dBm, 15 dBm, 19 dBm and 24 dBm being the thresholds at which 2, 4, 8, and 16-PIM outperform its base 4-QAM counterpart. For a transmission power of ≤ 50 dBm, $L \leq 8$ all manage to saturate, which is not achieved by 16-PIM. In order for 16-PIM to achieve its maximum data rate an even higher transmission power would be needed which is not realistic for a typical communication system. Therefore, the realistic upper limit to the number of bits modulated by PIM is 3 with 8-PIM.

In Fig. 12, the results are provided to observe 2-PIM with some commonly used higher orders of QAM. As expected, as modulation order increases the BER also increases. This is expected, as the higher the modulation order the greater the number of points on the constellation diagram. This results in points on the diagram being closer in proximity and therefore the chance of maximum-likelihood demodulation recognizing the wrong point is higher. The reason why QAM is used in these simulations over PSK is given in Section V-D.

D. Impact of Channel Parameters

The effect of CSI accuracy for a 4-QAM-PIM joint modulation is investigated in Fig. 13. We see that as the accuracy decreases, the BER increases. This is caused by the estimation not accounting for the correct changes to the signal as it passes through the channel. It can also be observed that a small drop in the CSI accuracy leads to a large increase in BER, outlining the importance of a good channel estimation algorithm.

Looking at the impact of channel estimation on data rate, Fig. 14 shows that ρ has a much larger impact on higher L modulation, with the transmission power needed to achieve saturation significantly higher for less accurate channels for 4-PIM compared to 2-PIM; going from 20 dBm to achieve saturation in a perfectly estimated channel compared to 30 dBm for $\rho = 0.995$ and $\rho = 0.99$ not achieving saturation. By contrast, there is roughly a 5 dBm range from a perfect CSI to a 99% accurate CSI for 2-PIM. This tells us that when the channel estimation is not very accurate, 2-PIM should be used instead of larger values of L due to the high drop-off for higher

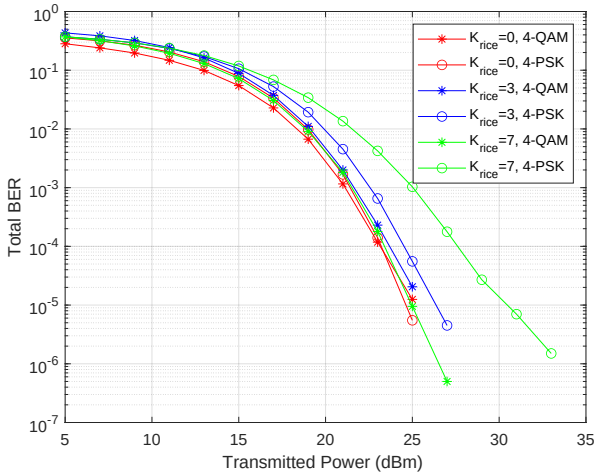

Fig. 15. Impact of Rice Factor on performance. All PSK and QAM modulations are done in conjunction with 4-PIM.

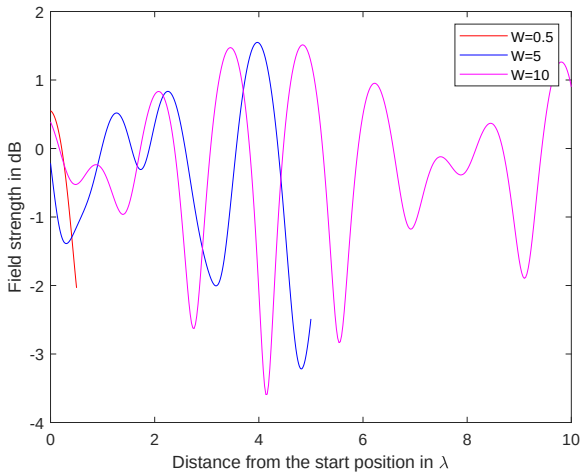

Fig. 16. The channel envelope with varying FAS sizes of 0.5λ, 5λ and 10λ.

PIM modulation. Furthermore, if a higher PIM modulation is used, after a transmission power of 30 dBm, any increase to transmission power leads to minimal gains in data rate and the transmission power can be kept at 30 dBm without significant losses to the performance of PIM. Additionally, the performance of SM under SM-P was compared to PIM. SM-P assumes perfect channel conditions and thus has channel estimation accuracy of $\rho = 1$. As we can see, PIM outperforms SM-P when the order of both modulations is two no matter the channel estimation accuracy. However for an order of 4, it can be seen that a perfectly estimated SM-P modulation will outperform PIM when the accuracy is $\rho = 0.99$ or lower.

Although CSI accuracy has impact on the performance of the proposed system, a high degree of CSI accuracy is realistic in many communication systems. It is possible to reduce the error of channel estimation below 10^{-2} as seen in [64], with more recent studies showing a channel accuracy of $\rho \geq 0.99$ being achievable even at low SNR of 10 [65].

Another significant channel consideration is the strength of the LoS path. During simulations, an assumption of $K_{\text{rice}} = 7$ was considered which represents a good LoS channel. However, this is not always the case in practice. Fig 15 looks at the impact of the strength of the LoS path by observing $K_{\text{rice}} = [0, 3, 7]$, where $K_{\text{rice}} = 0$ represents the NLoS case and therefore a Rayleigh channel. Accordingly, the performance of QAM seems similar for all values of K_{rice} while the performance of PSK increases as K_{rice} decreases. For a Rayleigh channel at $K_{\text{rice}} = 0$, PSK and QAM are observed to have a very similar performance. Therefore when the strength of the LoS path is high, QAM is the more reliable modulation to use in conjunction with PIM but in situations where there is low or no LoS, PSK is a viable alternative.

E. Impact of FAS Size and Number of Ports

As the FAS size increases, so does the space to the fluid antenna and access to a different signal envelope as can be seen in Fig. 16. However, with an increase in the size, for the same number of ports, the resolution effectively decreases due to the ports being spread out over a larger space. Fig. 17 shows that for QAM-PIM modulation, as the size of the fluid antenna increases, the BER decreases, reaching a saturation around $W = 25$. This is expected, as the more fading envelopes the fluid antenna has access to, the larger the range of phases and amplitudes between ports making the optimized port selection algorithm even more effective. However, PSK-PIM does not seem to show any significant trends based on the fluid antenna length. One possible reason for this could be that PSK relies on the precise changing of phases, and both the port selection algorithm and the increased length of the fluid antenna would change the phase of the signal, interfering with PSK. This once again shows that QAM is the preferred modulation to be used in conjunction with PIM. Furthermore, it can be seen that the number of ports does not have a significant impact on the BER below $W = 15$. This could be that even $N = 400$ ports, the resolution is still sufficient to obtain an accurate result. The results also illustrate that as W increases, the lack of resolution of $N = 400$ is starting to affect the BER, and that $N = 1400$, $N = 2400$ have similar BERs even at larger antenna sizes due to them having sufficient resolution.

F. Impact of Scatterers

The number of scatterers in the environment varies depending on the scenario, and so the impact of scatterers needs to be considered. In Fig. 18, we observe that as the number of scatterers increases, the variation in the channel envelope also increases. In theory, this is desirable for FAS due to the natural ability for fluid antennas to take advantage of more spatial diversity. For PIM, having a rich scattering environment is also desirable because having larger channel variations means that the optimal port selection algorithm will have a larger range to select from. The results in Fig. 19 indicate that the BER decreases significantly with the number of scatterers until $N_{\text{p}} = 2$, after which the BER seems to fluctuate and not have any clear correlation with the number of scatterers. This could be because after $N_{\text{p}} = 2$, the number of scatterers in the

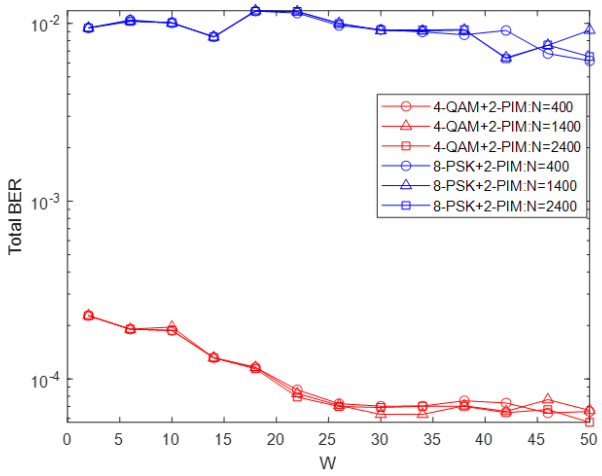

Fig. 17. Impact of FAS size and port number on BER.

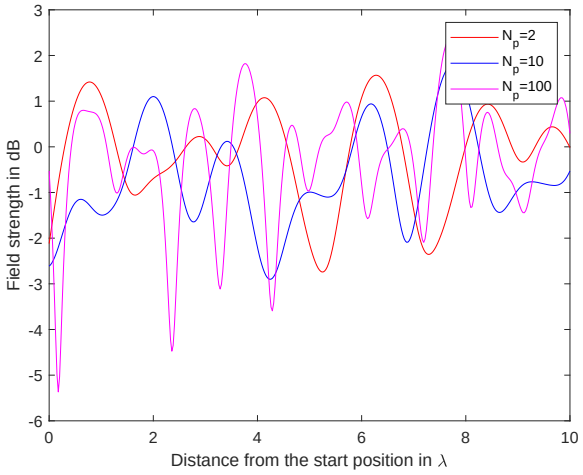

Fig. 18. The channel envelope with different numbers of scatterers.

environment is already sufficient to produce a varied enough channel for optimal port selection to take advantage of.

VI. Conclusion

This paper has the novel proposition of using fluid antennas at the transmitter (base station) as opposed to existing work which solely focuses on FAS at the receiver side. By doing this, it is possible to implement a new type of index modulation scheme by grouping ports on a fluid antenna and assigning a different index to each port group. Similar to all forms of modulation, as the number of bits modulated by PIM increases the signal quality deteriorates. In situations where the channel is good or the demands on QoS in terms of BER are not high (for example in semantic communications or non ultra-reliable scenarios), increasing the number of bits modulated could have an overall advantage. To maximize the effectiveness of PIM, a new port selection algorithm was proposed that maximizes the Euclidean distance between the selected port for each group. Also, a new transceiver architecture was proposed to implement PIM in conjunction with an existing modulation

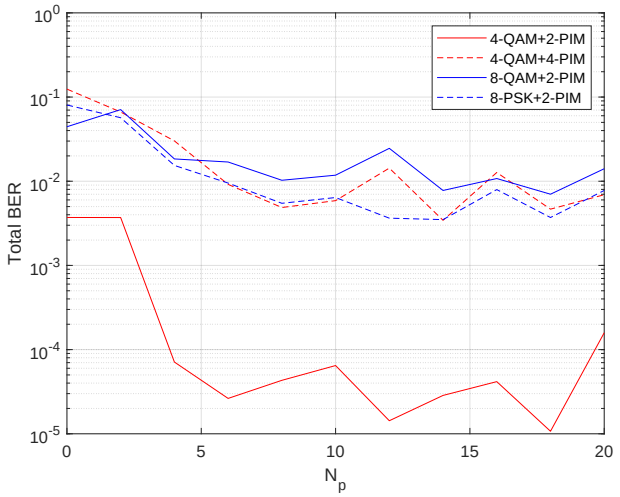

Fig. 19. BER with different number of scatterers for different modulations.

scheme like PSK or QAM. Expressions for BER and data rate were derived to analyze the performance of the proposed joint modulation. Numerical analysis has shown the impact of parameters such as channel estimation accuracy, different number of bits modulated by PIM and antenna size and port number on the BER and data rate of a communication system utilizing PIM. Furthermore, the effectiveness of the proposed PIM algorithm has been verified. Our results showed that there is a saturation point on the achievable data rate for both transmission power and port number, going beyond which will have little effect on the system performance. This insight is critical for system designers to optimize their designs.

Future work in this direction could involve observing a system where both the transmitter and receiver posses a fluid antenna. In this situation, the modulation process would be significantly more complicated as the transmitter would need to know the location of the active port on the receiver before accurate modulation can occur and a joint port selection algorithm would need to be devised that achieves a high degree of accuracy but also is not too computationally intensive.

Appendix A

For any two complex numbers $a \in \mathbb{C}$ and $b \in \mathbb{C}$, we have

$$\begin{aligned}
&|a^2+b^2| \\
=&[\mathrm{Re}\{a\}+\mathrm{Re}\{b\}]^2+[\mathrm{Im}\{a\}+\mathrm{Im}\{b\}]^2 \\
=&\mathrm{Re}^2\{a\}+2\mathrm{Re}\{a\}\mathrm{Re}\{b\}+\mathrm{Re}^2\{b\}+\mathrm{Im}^2\{a\} \\
&+2\mathrm{Im}\{a\}\mathrm{Im}\{b\}+\mathrm{Im}^2\{b\} \\
=&\mathrm{Re}^2\{a\}+\mathrm{Im}^2\{a\}+\mathrm{Re}^2\{b\}+\mathrm{Im}^2\{b\} \\
&+2\mathrm{Re}\{a\}\mathrm{Re}\{b\}+2\mathrm{Im}\{a\}\mathrm{Im}\{b\} \\
=&|a|^2+|b|^2+2\mathrm{Re}\{a\}\mathrm{Re}\{b\}+2\mathrm{Im}\{a\}\mathrm{Im}\{b\}. \qquad (25)
\end{aligned}$$

Since

$$\begin{aligned} ab^* =& \left(\mathrm{Re}\{a\}+j\mathrm{Im}\{a\}\right)\left(\mathrm{Re}\{b\}-j\mathrm{Im}\{b\}\right) \\ =&\mathrm{Re}\{a\}\mathrm{Re}\{b\}-j\mathrm{Re}\{a\}\mathrm{Im}\{b\} \\ &+j\mathrm{Im}\{a\}\mathrm{Re}\{b\}+\mathrm{Im}\{a\}\mathrm{Im}\{b\} \\ =&\mathrm{Re}\{a\}\mathrm{Re}\{b\}+\mathrm{Im}\{a\}\mathrm{Im}\{b\} \\ &+j\left(\mathrm{Im}\{a\}\mathrm{Re}\{b\}-\mathrm{Re}\{a\}\mathrm{Im}\{b\}\right), \end{aligned} \tag{26}$$

we know that

$$\mathrm{Re}\{ab^*\}=\mathrm{Re}\{a\}\mathrm{Re}\{b\}+\mathrm{Im}\{a\}\mathrm{Im}\{b\}. \tag{27}$$

Then (25) can be simplified as

$$|a^2+b^2|=|a|^2+|b|^2+2\mathrm{Re}\{ab^*\}. \tag{28}$$

Applying (28) to (12), we obtain

$$\begin{aligned} &\Pr\left[|(\rho-1)g_l b_m+\lambda_{m,l}|^2>|\rho g_l b_m-g_p b_n+\lambda_{m,l}|^2\right] \\ =&\Pr[|(\rho-1)g_l b_m|^2+|\lambda_{m,l}|^2+2\mathrm{Re}\{\lambda_{m,l}[(\rho-1)g_l b_m]^*\} \\ >&|\lambda_{m,l}|^2+|\rho g_l b_m-g_p b_n|^2+2\mathrm{Re}\{\lambda_{m,l}[\rho g_l b_m-g_p b_n]^*\}] \\ =&\Pr[2\mathrm{Re}\{\lambda_{m,l}[(\rho-1)g_l b_m]^*\}-2\mathrm{Re}\{\lambda_{m,l}[\rho g_l b_m-g_p b_n]^*\} \\ >&|\rho g_l b_m-g_p b_n|^2-|(\rho-1)g_l b_m|^2] \\ =&\Pr[2\mathrm{Re}\{\lambda_{m,l}(g_p b_n-g_l b_m)^*\} \\ >&|\rho g_l b_m-g_p b_n|^2-|(\rho-1)g_l b_m|^2]. \end{aligned} \tag{29}$$

REFERENCES

[1] X. You *et al.*, "Toward 6G TKμ extreme connectivity: Architecture, key technologies and experiments," *IEEE Wireless Commun.*, vol. 30, no. 3, pp. 86–95, Jun. 2023.

[2] X. Zhang and Q. Zhu, "AI-enabled network-functions virtualization and software-defined architectures for customized statistical QoS over 6G massive MIMO mobile wireless networks," *IEEE Netw.*, vol. 37, no. 2, pp. 30–37, Mar./Apr. 2023.

[3] C. Huang, A. Zappone, G. C. Alexandropoulos, M. Debbah and C. Yuen, "Reconfigurable intelligent surfaces for energy efficiency in wireless communication," *IEEE Trans. Wireless Commun.*, vol. 18, no. 8, pp. 4157–4170, Aug. 2019.

[4] Y. Liu *et al.*, "Developing NOMA to next generation multiple access: Future vision and research opportunities," *IEEE Wireless Commun.*, vol. 29, no. 6, pp. 120–127, Dec. 2022.

[5] K. K. Wong, A. Shojaeifard, K. F. Tong, and Y. Zhang, "Fluid antenna systems," *IEEE Trans. Wireless Commun.*, vol. 20, no. 3, pp. 1950–1962, Mar. 2021.

[6] Y. Shen, K. F. Tong, and K. K. Wong, "Reconfigurable surface wave fluid antenna for spatial MIMO applications," in *Proc. IEEE-APS Topical Conf. Antennas and Propag. Wireless Commun. (APWC)*, pp. 150–152, 9-13 Aug. 2021, Honoluli, HI, USA.

[7] B. A. Cetiner *et al.*, "Multifunctional reconfigurable MEMS integrated antennas for adaptive MIMO systems," *IEEE Commun. Mag.*, vol. 42, pp. 62–71, Dec. 2004.

[8] Y. Zhang, Z. Han, S. Tang, S. Shen, C. -Y. Chiu and R. Murch, "A highly pattern-reconfigurable planar antenna with 360° single- and multi-beam steering," *IEEE Trans. Antennas & Propag.*, vol. 70, no. 8, pp. 6490–6504, Aug. 2022.

[9] T. V. Hoang, V. Fusco, M. A. B. Abbasi, and O. Yurduseven, "Single-pixel polarimetric direction of arrival estimation using programmable coding metasurface aperture," *Nature, Sci. Rep.*, vol. 11, no. 23830, Dec. 2021.

[10] Y. Shen *et al.*, "Design and implementation of mmWave surface wave enabled fluid antennas and experimental results for fluid antenna multiple access," *arXiv preprint*, arXiv:2405.09663, May 2024.

[11] J. Zhang *et al.*, "A pixel-based reconfigurable antenna design for fluid antenna systems," *arXiv preprint*, arXiv:2406.05499, Jun. 2024.

[12] S. Dash, C. Psomas, and I. Krikidis, "Selection of metallic liquid in sub-6 GHz antenna design for 6G networks," *Nature Sci. Rep.*, vol. 13, no. 20551, 2023.

[13] T. Qiao *et al.*, "Pixel antenna optimization using the adjoint method and the method of moving asymptote," *IEEE Trans. Antennas & Propag.*, vol. 71, no. 3, pp. 2873–2878, Mar. 2023.

[14] W. Zheng and H. Li, "Designing antennas with quasi-isotropic radiation patterns using pixel structures," *IEEE Trans. Antennas & Propag.*, vol. 71, no. 10, pp. 7813–7823, Oct. 2023.

[15] L. Zhu, and K. K. Wong, "Historical review of fluid antennas and movable antennas," *arXiv preprint*, arXiv:2401.02362v2, Jan. 2024.

[16] M. Khammassi, A. Kammoun and M.-S. Alouini, "A new analytical approximation of the fluid antenna system channel," *IEEE Trans. Wireless Commun.*, vol. 22, no. 12, pp. 8843–8858, Dec. 2023.

[17] C. Psomas, P. J. Smith, H. A. Suraweera and I. Krikidis, "Continuous fluid antenna systems: Modeling and analysis," *IEEE Commun. Lett.*, vol. 27, no. 12, pp. 3370–3374, Dec. 2023.

[18] C. Psomas, G. M. Kraidy, K. K. Wong and I. Krikidis, "On the diversity and coded modulation design of fluid antenna systems," *IEEE Trans. Wireless Commun.*, vol. 23, no. 3, pp. 2082–2096, Mar. 2024.

[19] J. D. Vega-Sánchez, A. E. López-Ramírez, L. Urquiza-Aguiar and D. P. M. Osorio, "Novel expressions for the outage probability and diversity gains in fluid antenna system," *IEEE Wireless Commun. Lett.*, vol. 13, no. 2, pp. 372–376, Feb. 2024.

[20] W. K. New, K. K. Wong, H. Xu, K. F. Tong and C.-B. Chae, "Fluid antenna system: New insights on outage probability and diversity gain," *IEEE Trans. Wireless Commun.*, vol. 23, no. 1, pp. 128–140, Jan. 2024.

[21] L. Tlebaldiyeva, G. Nauryzbayev, S. Arzykulov, A. Eltawil and T. Tsiftsis, "Enhancing QoS through fluid antenna systems over correlated Nakagami-m fading channels," in *Proc. IEEE Wireless Commun. Netw. Conf. (WCNC)*, pp. 78–83, 10-13 Apr. 2022, Austin, TX, USA.

[22] J. D. Vega-Sánchez, L. Urquiza-Aguiar, M. C. P. Paredes and D. P. M. Osorio, "A simple method for the performance analysis of fluid antenna systems under correlated Nakagami-m fading," *IEEE Wireless Commun. Lett.*, vol. 13, no. 2, pp. 377–381, Feb. 2024.

[23] P. D. Alvim *et al.*, "On the performance of fluid antennas systems under α-μ fading channels," *IEEE Wireless Commun. Lett.*, vol. 13, no. 1, pp. 108–112, Jan. 2024.

[24] F. R. Ghadi, K. K. Wong, F. J. López-Martínez and K. F. Tong, "Copula-based performance analysis for fluid antenna systems under arbitrary fading channels," *IEEE Commun. Lett.*, vol. 27, no. 11, pp. 3068–3072, Nov. 2023.

[25] Y. Hou *et al.*, "A copula-based approach to performance analysis of fluid antenna system with multiple fixed transmit antennas," *IEEE Wireless Commun. Lett.*, vol. 13, no. 2, pp. 501–504, Feb. 2024.

[26] L. Tlebaldiyeva, S. Arzykulov, K. M. Rabie, X. Li and G. Nauryzbayev, "Outage performance of fluid antenna system (FAS)-aided terahertz communication networks," in *Proc. IEEE Inter. Conf. Commun.*, pp. 1922–1927, 28 May-1 Jun. 2023, Rome, Italy.

[27] X. Lai *et al.*, "On performance of fluid antenna system using maximum ratio combining," *IEEE Commun. Lett.*, vol. 28, no. 2, pp. 402–406, Feb. 2024.

[28] W. K. New, K. K. Wong, H. Xu, K. F. Tong and C.-B. Chae, "An information-theoretic characterization of MIMO-FAS: Optimization, diversity-multiplexing tradeoff and q-outage capacity," *IEEE Trans. Wireless Commun.*, vol. 23, no. 6, pp. 5541–5556, Jun. 2024.

[29] C. Skouroumounis and I. Krikidis, "Fluid antenna with linear MMSE channel estimation for large-scale cellular networks," *IEEE Trans. Commun.*, vol. 71, no. 2, pp. 1112–1125, Feb. 2023.

[30] H. Xu *et al.*, "Channel estimation for FAS-assisted multiuser mmWave systems," *IEEE Commun. Lett.*, vol. 28, no. 3, pp. 632–636, Mar. 2024.

[31] Z. Zhang, J. Zhu, L. Dai, and R. W. Heath Jr, "Successive Bayesian reconstructor for channel estimation in fluid antenna systems," *arXiv preprint*, arXiv:2312.06551v3, 2024.

[32] C. Psomas, G. M. Kraidy, K. K. Wong and I. Krikidis, "Fluid antenna systems with outdated channel estimates," in *Proc. IEEE Inter. Conf. Commun. (ICC)*, pp. 2970–2975, 28 May-1 Jun. 2023, Rome, Italy.

[33] J. Zou, S. Sun and C. Wang, "Online learning-induced port selection for fluid antenna in dynamic channel environment," *IEEE Wireless Commun. Lett.*, vol. 13, no. 3, pp. 313–317, Feb. 2024.

[34] Y. Ye *et al.*, "Fluid antenna-assisted MIMO transmission exploiting statistical CSI," *IEEE Commun. Lett.*, vol. 28, no. 1, pp. 223–227, Jan. 2024.

[35] C. Skouroumounis and I. Krikidis, "Fluid antenna-aided full duplex communications: A macroscopic point-of-view," *IEEE J. Select. Areas Commun.*, vol. 41, no. 9, pp. 2879–2892, Sept. 2023.

[36] K. K. Wong, D. Morales-Jimenez, K. F. Tong, and C. B. Chae, "Slow fluid antenna multiple access," *IEEE Trans. Commun.*, vol. 71, no. 5, pp. 2831–2846, May 2023.

[37] H. Yang, K. K. Wong, K. F. Tong, Y. Zhang, and C. B. Chae, "Performance analysis of slow fluid antenna multiple access in noisy channels using Gauss-Laguerre and Gauss-Hermite quadratures," *IEEE Commun. Lett.*, vol. 27, no. 7, pp. 1734–1738, Jul. 2023.
[38] Y. Chen, S. Li, Y. Hou and X. Tao, "Energy-efficiency optimization for slow fluid antenna multiple access using mean-field game," *IEEE Wireless Commun. Lett.*, vol. 13, no. 4, pp. 915–918, Apr. 2024.
[39] K. K. Wong and K. F. Tong, "Fluid antenna multiple access," *IEEE Trans. Wireless Commun.*, vol. 21, no. 7, pp. 4801–4815, Jul. 2022.
[40] K. K. Wong, K. F. Tong, Y. Chen, and Y. Zhang, "Fast fluid antenna multiple access enabling massive connectivity," *IEEE Commun. Lett.*, vol. 27, no. 2, pp. 711–715, Feb. 2023.
[41] L. Tlebaldiyeva, S. Arzykulov, T. A. Tsiftsis and G. Nauryzbayev, "Full-duplex cooperative NOMA-based mmWave networks with fluid antenna system (FAS) receivers," in *Proc. Inter. Balkan Conf. Commun. Netw. (BalkanCom)*, pp. 1–6, 5-8 Jun. 2023, Istanbul, Turkey.
[42] W. K. New *et al.*, "Fluid antenna system enhancing orthogonal and non-orthogonal multiple access," *IEEE Commun. Lett.*, vol. 28, no. 1, pp. 218–222, Jan. 2024.
[43] F. R. Ghadi *et al.*, "Fluid antenna-assisted dirty multiple access channels over composite fading," *IEEE Commun. Lett.*, vol. 28, no. 2, pp. 382–386, Feb. 2024.
[44] K. K. Wong, C. B. Chae and K. F. Tong, "Compact ultra massive antenna array: A simple open-loop massive connectivity scheme," *IEEE Trans. Wireless Commun.*, vol. 23, no. 6, pp. 6279–6294, Jun. 2024.
[45] A. A. Purwita, A. Yesilkaya, M. Safari, and H. Haas, "Generalized time slot index modulation for optical wireless communications," *IEEE Trans. Commun.*, vol. 68, no. 6, pp. 3706–3719, Jun. 2020.
[46] A. A. Purwita, A. Yesilkaya, T. Cogalan, M. Safari, and H. Haas, "Generalized time slot index modulation for LiFi," in *Proc. IEEE Inter. Symp. Pers., Indoor Mobile Radio Commun. (PIMRC)*, 8-11 Sept. 2019, Istanbul, Turkey.
[47] L. N. Theagarajan, "Multi-mode generalized space-time index modulation: A high-rate index modulation scheme for MIMO-ISI channels," in *Proc. IEEE Global Conf. Signal Inf. Proc. (GlobalSIP)*, 11-14 Nov. 2019, Ottawa, Canada.
[48] E. Aydin and H. Ilhan, "A novel SM-based MIMO system with index modulation," *IEEE Commun. Lett.*, vol. 20, no. 2, pp. 244–247, Feb. 2016.
[49] M. Wen, X. Cheng, and L. Yang, "Index Modulation for 5G Wireless Communications," *Cham: Springer International Publishing*, 2017.
[50] E. Basar, M. Wen, R. Mesleh, M. Di Renzo, Y. Xiao and H. Haas, "Index Modulation Techniques for Next-Generation Wireless Networks," *IEEE Access*, vol. 5, pp. 16693–16746, Aug 2017.
[51] E. Basar, "Reconfigurable intelligent surface-based index modulation: A new beyond MIMO paradigm for 6G," *IEEE Trans. Commun.*, vol. 68, no. 5, pp. 3187–3196, May 2020.
[52] Y. Hussein, M. Assaad, and H. Sari, "Reconfigurable intelligent surface index modulation with signature constellations," in *Proc. IEEE Wireless Commun. Netw. Conf. (WCNC)*, 29 Mar.-1 Apr. 2021, Nanjing, China.
[53] R. Singh *et al.*, "Indexed multiple access with reconfigurable intelligent surfaces: The reflection tuning potential," *arXiv preprint*, arXiv:2302.07476, 2023.
[54] J. Zhu *et al.*, "Index modulation for fluid antenna-assisted MIMO communications: System design and performance analysis," *IEEE Trans. Wireless Commun.*, early access, DOI:10.1109/TWC.2024.3364712, Feb 2024.
[55] H. S. Hussein and M. Hagag, "Optical MIMO-OFDM with fully generalized index-spatial LED modulation," *IEEE Commun. Lett.*, vol. 23, no. 9, pp. 1556–1559, Sept. 2019.
[56] M. D. Renzo, H. Haas, A. Ghrayeb, S. Sugiura and L. Hanzo, "Spatial modulation for generalized MIMO: challenges, opportunities, and implementation " *Proc. IEEE*, vol. 102, no. 1, pp. 56–103, Jan. 2014.
[57] Y. Chau and S. H. Yu, "Space modulation on wireless fading channels," in *Proc. IEEE Veh. Technol. Conf. Fall,*, vol. 3, pp. 1668–1671, 7-11 Oct. 2001, Atlantic City, NJ, USA.
[58] M. D. Renzo and H. Haas, "Improving the performance of space shift keying (SSK) modulation via opportunistic power allocation," *IEEE Commun. Lett.*, vol. 14, pp. 500–502, Jun. 2010.
[59] H. Albinsaid, K. Singh, S. Biswas, C. -P. Li and M. -S. Alouini, "Block deep neural network-based signal detector for generalized spatial modulation," *IEEE Commun. Lett.*, vol. 24, no. 12, pp. 2775–2779, Dec. 2020.
[60] R. Mesleh, M. Di Renzo, H. Haas and P. M. Grant, "Trellis coded spatial modulation," *IEEE Trans. Wireless Commun.*, vol. 9, no. 7, pp. 2349–2361, Jul. 2010.
[61] M. D. Renzo and H. Haas, "Bit error probability of space modulation over Nakagami-m fading: Asymptotic analysis," *IEEE Commun. Lett.*, vol. 15, no. 10, pp. 1026–1028, Oct. 2011.
[62] Y. Zhao, J. Hu, A. Xie, K. Yang, and K. K. Wong, "Receive spatial modulation aided simultaneous wireless information and power transfer with finite alphabet," *IEEE Trans. Wireless Commun.*, vol. 19, no. 12, pp. 8039–8053, Dec. 2020.
[63] C. Masouros, "Improving the diversity of spatial modulation in MISO channels by phase alignment," *IEEE Commun. Lett.*, vol. 18, no. 5, pp. 729–732, May 2014.
[64] J. -J. van de Beek, O. Edfors, M. Sandell, S. K. Wilson and P. O. Borjesson, "On channel estimation in OFDM systems," in *Proc. IEEE Veh. Technol. Conf. (VTC)*, vol. 2, pp. 815–819, 25-28 July 1995, Chigaco, IL, USA.
[65] J. Mountassir, D. H. Mihai and D. Isar, "Improving the channel estimation accuracy for orthogonal modulation communication systems using denoising," in *Proc. Int. Symp. Elec. Telecomm. (ISETC)*, pp. 1–4, 14-15 Nov. 2014, Timisoara, Romania.
[66] E. Faddoul, G.M. Kraidy, C. Psomas and I. Krikidis, "Advanced channel coding designs for index-modulated fluid antenna systems," *arXiv preprint*, arXiv:2403.06839, 2024.
[67] D. Tse and P. Viswanath, "Fundamentals of Wireless Communication," *Cambridge UP: Cambridge*, 2013.

Halvin H. Yang received the B.Eng. degree in Electronic and Electrical Engineering from Imperial College London in 2020. He is currently doing a PhD degree for Electronic and Electrical Engineering in University College London starting in 2020. His research interests include resource allocation for edge communications and performance analysis of new 6G technologies like reconfigurable reflecting surfaces (RIS) and fluid antenna communication systems.

Hao Xu (S'15-M'19) received the B.S. degree in communication engineering from Nanjing University of Science and Technology, Nanjing, China, in 2013, and the Ph.D. degree in information and communication engineering with the National Mobile Communications Research Laboratory, Southeast University, Nanjing, China, in 2019. From 2019 to 2021, he was an Alexander von Humboldt (AvH) Post-Doctoral Research Fellow with the Faculty of Electrical Engineering and Computer Science at the Technical University of Berlin, Germany. He is currently a Marie Sk?odowska-Curie Actions (MSCA) Individual Fellow with the Department of Electronic and Electrical Engineering, University College London, UK. His research interests mainly include information theory, mathematical optimization, MIMO systems, fluid antenna systems, and physical layer security in wireless networks.

(Kit) Kai-Kit Wong (M'01-SM'08-F'16) received the BEng, the MPhil, and the PhD degrees, all in Electrical and Electronic Engineering, from the Hong Kong University of Science and Technology, Hong Kong, in 1996, 1998, and 2001, respectively. After graduation, he took up academic and research positions at the University of Hong Kong, Lucent Technologies, Bell-Labs, Holmdel, the Smart Antennas Research Group of Stanford University, and the University of Hull, UK. He is Chair in Wireless Communications at the Department of Electronic and Electrical Engineering, University College London, UK.

His current research centers around 5G and beyond mobile communications. He is a co-recipient of the 2013 IEEE Signal Processing Letters Best Paper Award and the 2000 IEEE VTS Japan Chapter Award at the IEEE Vehicular Technology Conference in Japan in 2000, and a few other international best paper awards. He is Fellow of IEEE and IET and is also on the editorial board of several international journals. He served as the Editor-in-Chief for IEEE Wireless Communications Letters between 2020 and 2023.

Chan-Byoung Chae (S'06-M'09-SM'12-F'21) is an Underwood Distinguished Professor in the School of Integrated Technology, Yonsei University, Korea. Before joining Yonsei University, he was with Bell Labs, Alcatel-Lucent, Murray Hill, NJ, USA from 2009 to 2011, as a Member of Technical Staff, and Harvard University, Cambridge, MA, USA from 2008 to 2009, as a Postdoctoral Research Fellow. He received his Ph.D. degree in Electrical & Computer Engineering from The University of Texas at Austin in 2008. Prior to joining UT, he was a research engineer at the Telecommunications R&D Center, Samsung Electronics, Suwon, Korea, from 2001 to 2005.

He has been an Editor-in-Chief of the IEEE Trans. Molecular, Biological, and Multi-scale Communications (2019-2022) and a Senior Editor of the IEEE Wireless Communications Letters (2020-present). He has served/serves as an Editor for the IEEE Communications Magazine (2016-present), the IEEE Trans. on Wireless Communications (2012-2017), and the IEEE Wireless Communications Letters (2016-present). He is an IEEE ComSoc Distinguished Lecturer for the term 2020-2021 and 2022-2023.

He was the recipient/co-recipient of the CES Innovation Award in 2023, the IEEE ICC Best Demo Award in 2022, the IEEE WCNC Best Demo Award in 2020, the Best Young Engineer Award from the National Academy of Engineering of Korea (NAEK) in 2019, the IEEE DySPAN Best Demo Award in 2018, the IEEE/KICS Journal of Communications and Networks Best Paper Award in 2018, the IEEE INFOCOM Best Demo Award in 2015, the IEIE/IEEE Joint Award for Young IT Engineer of the Year in 2014, the KICS Haedong Young Scholar Award in 2013, the IEEE Signal Processing Magazine Best Paper Award in 2013, the IEEE ComSoc AP Outstanding Young Researcher Award in 2012, the IEEE VTS Dan. E. Noble Fellowship Award in 2008.

Ross Murch (S'84-M'90-SM'98-F'09) received the bachelor?s and Ph.D. degrees in electrical and electronic engineering from the University of Canterbury, Christchurch, New Zealand.

He is currently a Chair Professor in the Department of Electronic and Computer Engineering and a Senior Fellow at the Institute of Advanced Study both at the Hong Kong University of Science and Technology (HKUST). He is known for his research on multiple antenna technology including multiuser-MIMO, compact multiport antennas and multiport energy harvesting. His current research focus is creating new RF wave technology for making a better world and this includes RF imaging, ambient RF systems, energy harvesting, electromagnetic information theory, 6G, IoT, multiport antenna systems and reconfigurable intelligent surfaces. His unique expertise lies in his combination of knowledge from both wireless communication systems and electromagnetics and he publishes in both areas. In total his research contributions include over 200 journal publications and more than 20 patents while successfully supervising more than 50 research students. Professor Murch also has a strong interest in education, enjoys teaching and has won five teaching awards.

Prof. Murch was Department Head at HKUST from 2009-2015, is an IEEE, IET, HKIE, and FHKEng Fellow. He has been a David Bensted Fellow, Simon Fraser University, Canada, an HKTIIT fellow at Southampton University, U.K and has spent sabbaticals at MIT, USA; AT&T, USA; Allgon Mobile Communications, Sweden; Imperial College London. He was awarded the IEEE Communications Society Wireless Communications Technical Committee Recognition Award in 2023. He has served IEEE in various positions including IEEE area editor, technical program chair, distinguished lecturer and Fellow evaluation committee.

Professor Ross Murch joined HKUST in 1992 as an Assistant Professor and has remained at HKUST in Hong Kong since then, where he is now a Chair Professor. From 1990-1992 he was a Post-Doctoral Fellow at the Department of Mathematics and Computer Science, University of Dundee, UK.

Shi Jin (S?06-M?07-SM?17-F?24) received the B.S. degree in communications engineering from Guilin University of Electronic Technology, Guilin, China, in 1996, the M.S. degree from Nanjing University of Posts and Telecommunications, Nanjing, China, in 2003, and the Ph.D. degree in information and communications engineering from the Southeast University, Nanjing, in 2007. From June 2007 to October 2009, he was a Research Fellow with the Adastral Park Research Campus, University College London, London, U.K. He is currently with the faculty of the National Mobile Communications Research Laboratory, Southeast University. His research interests include wireless communications, random matrix theory, and information theory. He is serving as an Area Editor for the Transactions on Communications and IET Electronics Letters. He was an Associate Editor for the IEEE Transactions on Wireless Communications, and IEEE Communications Letters, and IET Communications. Dr. Jin and his co-authors have been awarded the 2011 IEEE Communications Society Stephen O. Rice Prize Paper Award in the field of communication theory, the IEEE Vehicular Technology Society 2023 Jack Neubauer Memorial Award, a 2022 Best Paper Award and a 2010 Young Author Best Paper Award by the IEEE Signal Processing Society.

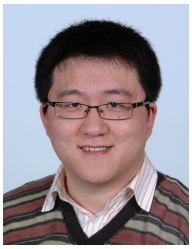

Yangyang Zhang received the B.S. and M.S. degrees in electronics and information engineering from Northeastern University, Shenyang, China, in 2002 and 2004 respectively, and the Ph.D. degree in electrical engineering from the University of Oxford, Oxford, U.K., in 2008.

He is currently taking the position of Executive Director of Kuang-Chi Science Limited, Hong Kong. His research interests include multiple-input multiple-output wireless communications and stochastic optimization algorithms. Dr. Zhang has been awarded more than 20 honors. Besides, he also authored and co-authored more than 40 refereed papers.